Journal of
Synchrotron
Radiation

ISSN 0909-0495

Received 6 December 2011
Accepted 21 April 2012

The first microbeam synchrotron X-ray fluorescence beamline at the Siam Photon Laboratory

Somchai Tancharakorn,[a]* Waraporn Tanthanuch,[a] Nuntaporn Kamonsutthipaijit,[a] Narupon Wongprachanukul,[a] Methee Sophon,[a] Sarunyu Chaichuay,[a] Chunmanus Uthaisar[a] and Rattikorn Yimnirun[b]

[a]Synchrotron Light Research Institute (Public Organization), 111 University Avenue, Muang District, Nakhon-Ratchasima 30000, Thailand, and [b]School of Physics, Institute of Science, Suranaree University of Technology, University Avenue, Muang District, Nakhon-Ratchasima 30000, Thailand. E-mail: somchai@slri.or.th

The first microbeam synchrotron X-ray fluorescence (μ-SXRF) beamline using continuous synchrotron radiation from Siam Photon Source has been constructed and commissioned as of August 2011. Utilizing an X-ray capillary half-lens allows synchrotron radiation from a 1.4 T bending magnet of the 1.2 GeV electron storage ring to be focused from a few millimeters-sized beam to a micrometer-sized beam. This beamline was originally designed for deep X-ray lithography (DXL) and was one of the first two operational beamlines at this facility. A modification has been carried out to the beamline in order to additionally enable μ-SXRF and synchrotron X-ray powder diffraction (SXPD). Modifications included the installation of a new chamber housing a Si(111) crystal to extract 8 keV synchrotron radiation from the white X-ray beam (for SXPD), a fixed aperture and three gate valves. Two end-stations incorporating optics and detectors for μ-SXRF and SXPD have then been installed immediately upstream of the DXL station, with the three techniques sharing available beam time. The μ-SXRF station utilizes a polycapillary half-lens for X-ray focusing. This optic focuses X-ray white beam from 5 mm × 2 mm (H × V) at the entrance of the lens down to a diameter of 100 μm FWHM measured at a sample position 22 mm (lens focal point) downstream of the lens exit. The end-station also incorporates an *XYZ* motorized sample holder with 25 mm travel per axis, a 5× ZEISS microscope objective with 5 mm × 5 mm field of view coupled to a CCD camera looking to the sample, and an AMPTEK single-element Si (PIN) solid-state detector for fluorescence detection. A graphic user interface data acquisition program using the *LabVIEW* platform has also been developed in-house to generate a series of single-column data which are compatible with available XRF data-processing software. Finally, to test the performance of the μ-SXRF beamline, an elemental surface profile has been obtained for a piece of ancient pottery from the Ban Chiang archaeological site, a UNESCO heritage site. It was found that the newly constructed μ-SXRF technique was able to clearly distinguish the distribution of different elements on the specimen.

Keywords: microbeam synchrotron X-ray fluorescence; archaeological pottery.

1. Introduction

Energy-dispersive X-ray fluorescence provides a rapid analysis of multi-element detection in both a qualitative and quantitative approach. For more than half a century it has been considered as an effective user-friendly technique and therefore commonly used in laboratories around the world. Excellent reviews of this technique can be found by Kanngießer & Haschke (2006). Recently, owing to its high intensity and energy tunability, synchrotron radiation has become recognized as an ideal X-ray source for X-ray fluorescence (XRF) microspectroscopy compared with more conventional sources such as sealed-tube or rotating-anode generators. The high intensity of synchrotron X-ray-based instruments allows for very low elemental concentrations to be detected and analyzed. While conventional XRF spectroscopy is used for bulk chemical analysis of samples, assuming that composition is homogeneous, the high brightness of synchrotron sources

allows instruments to be constructed that produce micrometer-sized beams of X-rays for studying the microscopic properties of materials. These microfocused XRF techniques can provide information not only on the elemental compositions but also their distribution at the micrometer scale (Kanngießer & Haschke, 2006).

In order to provide a micrometer-sized X-ray beam, an optical focusing system is required. Several systems with different principles have been developed and are commercially available such as multilayer optics (Yanagihara & Yamashita, 2004) or parabolic compound refractive lenses (Lengeler *et al.*, 1999). We chose to utilize polycapillary X-rays owing to the ease of usage and cost effectiveness (Bilderback, 2007). Optical alignment of the capillary is achieved with the help of a motorized sample holder with three degrees of freedom. Beamlines designed to provide μ-XRF capabilities are found at virtually every synchrotron facility worldwide with applications in various research areas including materials science (Kempenaersa *et al.*, 2000), archaeology (Dumont *et al.*, 2009), medical science (Geraki *et al.*, 2004) and environmental science (Frisia *et al.*, 2005), to name a few.

This manuscript presents a new upgrade of an existing beamline to enable the microbeam synchrotron X-ray fluorescence (μ-SXRF) technique at the Siam Photon Laboratory (SPL) of the Synchrotron Light Research Institute (Public Organization) (SLRI), Nakhon Ratchasima, Thailand. This new capability provides SPL users with a new characterization technique. This beamline is the first beamline for XRF available in South-East Asia. Some technical details of the beamline and end-station, as well as its performances, will be presented and discussed here.

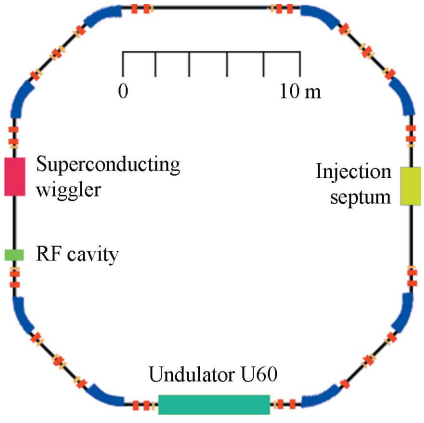

Figure 1
Schematic layout of the SPS storage ring.

2. Instrumentation

2.1. Synchrotron radiation source

The Siam Photon Source (SPS) at Nakhon Ratchasima, Thailand, consists of three main parts: a 40 MeV linear accelerator, a 1 GeV booster synchrotron and a 1.2 GeV electron storage ring. The X-ray storage ring utilizes a double-bend achromat lattice consisting of four periods with four straight sections for insertion devices. Each period has two bending magnets, four focusing quadrupole magnets and four defocusing quadrupole magnets. Therefore, at least eight beamlines can be accommodated. So far, one undulator with 60 periods (U60) of magnetic poles has been installed in one of the available straight sections. One superconducting wiggler will be installed in 2012. The layout of the magnet components and insertion devices in the SPS storage ring is shown in Fig. 1.

2.2. μ-SXRF beamline at the SPL

The original deep X-ray lithography (DXL) beamline has been upgraded and modified to accommodate three different techniques with the end-stations in a time-sharing arrangement. Components that were added as part of the upgrade include a fixed aperture made of an oxygen-free thermal conductivity copper, a water-cooled Si(111) crystal for fixed energy of 8 keV, a kapton window of thickness 50 μm installed at 7.7 m from the source, a turbomolecular pump with a desirable vacuum level of 10^{-6} torr, three gate valves and an interlock system, as displayed in Fig. 2.

The beamline utilizes a bending-magnet X-ray source. A beryllium window of thickness 100 μm is installed outside the radiation shielding wall. It is mainly used to separate ultra-high-vacuum and low-vacuum regions in the beamline. The beryllium window also acts as a low-energy filter, leaving continuous X-rays of energy above 2 keV to reach the end-stations. The fixed aperture reduces the beam size to 5 mm × 2 mm (H × V). A Si(111) crystal is then used to extract a monochromatic X-ray beam of 8 keV for X-ray diffraction experiments, *i.e.* synchrotron X-ray powder diffraction (SXPD). However, when this technique is not in operation, the crystal can be lifted up to allow continuous white-beam X-rays to reach other end-stations, *i.e.* μ-SXRF or DXL. Details of the SXPD end-station will not be discussed here. A μ-SXRF end-station sits upstream of the DXL end-station, but is designed to be replaced by a 1 m-long vacuum pipe when the DXL end-station is in operation. Three gate valves are employed to maintain vacuum environments during the vacuum duct replacement.

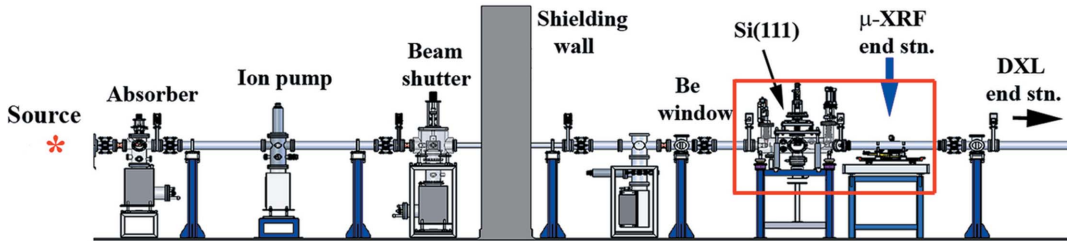

Figure 2
Optical components of the upgraded beamline for DXL, SXPD and μ-SXRF techniques at the SPL.

2.3. μ-SXRF end-station

The μ-SXRF end-station consists of four main components including an X-ray optical system, a visible-light microscope, a motorized sample holder with three degrees of freedom, and an energy-dispersive detection system, as shown in Fig. 3. In order to achieve a micrometer-sized beam, a focusing system for X-rays is essentially needed. Here, a polycapillary half-lens manufactured by UNISANTIS EUROPE GmbH is employed to focus an X-ray beam to the order of 100 μm in diameter. This polycapillary lens is installed on a motorized stage with four degrees of freedom. It is aligned using two linear motors with 6 μm precision and two rotational motors with 0.006° precision from MISUMI, Japan. A CCD camera coupled to a 5× ZEISS objective lens is also used to specify and capture the measured area of a sample. Motor precision for the sample stage is 1.5 μm with the sample surface sitting at the focal point of the polycapillary lens. All motor motions are remotely controlled. Detection of the X-ray fluorescence signal is *via* an energy-dispersive Si-PIN detector from AMPTEK, USA, with an active area of 13 mm^2 and energy resolution of 160 eV at the Mn K_α emission line. Energy-out signals from the detector are then registered at an MCA8000A multichannel analyzer (AMPTEK, USA) corresponding to the energy of X-rays.

2.4. Data acquisition program for μ-SXRF imaging

A data acquisition program using the *LabVIEW* platform has been developed at SPL. It is not only employed to acquire XRF data, but also to control three stepping motors for raster scanning the sample during the measurement. When the measurement is completed, a series of one-column XRF data files is generated. These stack files are compatible with most standard XRF analysis programs. However, the *ROI* image tool program of the *pyMCA* package is used here (Sole *et al.*, 2007). An image showing elemental distribution can therefore be analyzed.

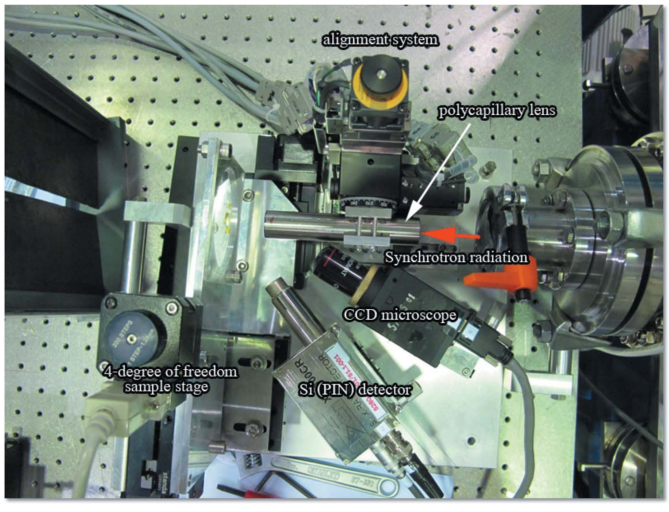

Figure 3
The μ-SXRF end-station.

3. Results and discussions

3.1. Beam profile

The beam size of the focused white beam has been measured to be 100 μm in the horizontal direction using a copper wire of diameter 10 μm. The wire is placed at the sample position where the distance between the polycapillary lens and sample is 22 mm (focal length of the polycapillary lens). The beam size measurement is carried out by measuring the intensity of Cu K_α X-ray fluorescence from the copper wire as a function of its position when scanned horizontally. The scanning step used here is 10 μm $step^{-1}$ and the exposure time is 15 s $step^{-1}$. The intensity of K_α X-rays from copper can be plotted as a function of position, and the beam size can be calculated using the following equation,

$$\oslash_{\rm beam} = \left({\rm FWHM}^2 - \oslash_{\rm wire}^2\right)^{1/2}, \quad (1)$$

where $\oslash_{\rm beam}$ and $\oslash_{\rm wire}$ are diameters of the X-ray beam and copper wire, respectively, and FWHM is the full width at half-maximum. Fig. 4 shows the data and the Gaussian function fitting of the intensity of Cu K_α X-rays as a function of horizontal position. Moreover, the beam size at different positions along the beam was also measured (see inset in Fig. 4). The central position is the focal point of the X-ray lens which is 22 mm, giving the smallest beam size of the X-ray beam.

3.2. Lower limit of detection

The lower limit of detection (LLD) is defined as the lowest quantity or intensity of the substance or element in a sample that can be detected. In practice, the LLD can be calculated statistically using the following equation (de Vries & Vrebos, 2002),

$${\rm LLD} = \frac{3C_i}{I_{\rm net}}\left(\frac{I_{\rm bg}}{T_{\rm bg}}\right)^{1/2}, \quad (2)$$

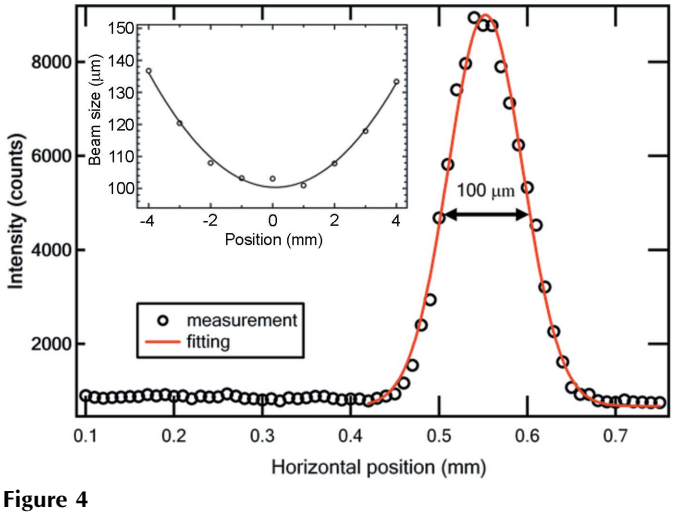

Figure 4
Intensity of Cu K_α X-rays as a function of horizontal position. Inset: beam size as a function of position along the beam axis.

Table 1
Lower level of detection (LLD) of the standard SRM610.

Element	Atomic number (Z)	C_i (p.p.m.)	LLD (p.p.m.)
Ti	22	437	8.3
V	23	500	6.8
Cr	24	500	5.1
Mn	25	485	4.0
Fe	26	458	2.5
Co	27	390	2.6
Ni	28	458.7	3.2
Cu	29	444	3.3
Zn	30	433	3.9

where C_i is the concentration of i element (measured in parts per million, p.p.m.), I_{net} is the net intensity (count s^{-1}), I_{bg} is the background intensity (count s^{-1}) and T_{bg} is the collecting time of the background measurement (s). However, LLD depends on several factors such as the sample preparation (thickness, surface, heterogeneity, *etc.*) and matrix effects (absorption and enhancement). Here, a trace element in a glass matrix (SRM610) of thickness 3 mm from the National Institute of Standards and Technology (NIST), USA, was excited by synchrotron radiation with an exposure time of 1000 s. Using *pyMCA*, I_{net} of the K emission lines and I_{bg} can be extracted, and LLD can be calculated using (2). Fig. 5 shows the LLD values in the range below 10 p.p.m. as a function of atomic number Z from Ti (Z = 22) to Zn (Z = 30). Values are shown in Table 1.

3.3. Performance

An archaeological sample, Ban Chiang ancient pottery, was selected to test the performance of the end-station. The Ban Chiang archaeological site, located in the north-east of Thailand, is a UNESCO heritage site which spans three periods of pottery: pre-metal, bronze and iron ages (Tanthanuch *et al.*, 2011). The sample used here belongs to the iron age pottery which has been found to have a distinctive red pigment on painted surfaces and exquisite designs. XRF analysis of this red shard was of interest in studying the element distribution to provide insight into what materials were used for slip painting.

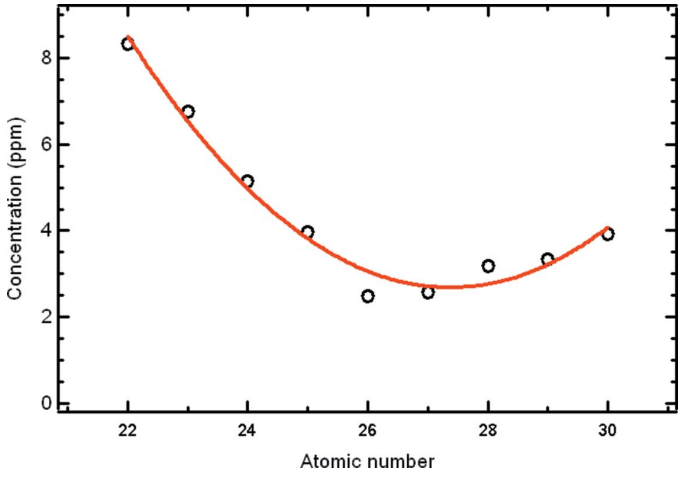

Figure 5
Lower level of detection of the standard SRM610 as a function of atomic number.

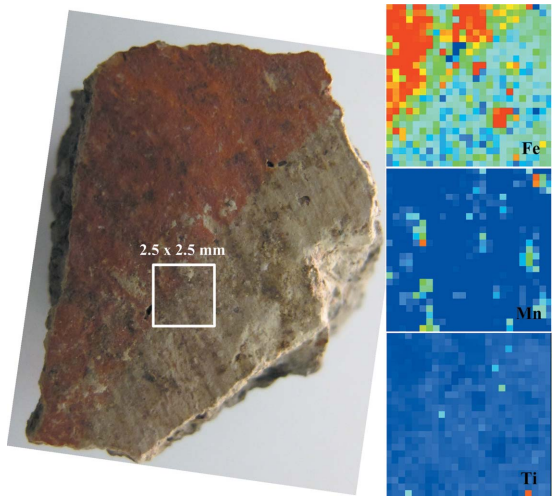

Figure 6
XRF images of a piece of Ban Chiang pottery showing the distribution of iron (Fe), manganese (Mn) and titanium (Ti) over an area of 2.5 mm × 2.5 mm.

An energy-dispersive XRF compositional map of one red painted shard is shown in Fig. 6. The map was produced in a step-scan mode and covers a 2.5 mm × 2.5 mm area in 100 µm steps and with 15 s dwell times per pixel. The area spans painted and unpainted portions of the pottery shard. The energy-dispersive data were then analyzed using the *ROI* image tool program in *pyMCA*. The distribution of three different elements (Fe, Mn and Ti) can be imaged with different false-color maps generated from an integrated area specific for each element. The colors red, green and blue represent high, medium and low intensities, respectively.

The results show that the distribution of iron (Fe) in the red painted area gives significantly higher counts consistent with elevated levels of Fe. Interestingly, the manganese (Mn) and titanium (Ti) distributions are not significantly different between painted and unpainted areas. This finding is in good agreement with McGovern *et al.* (1985) and Bubpha (2003), in which it has been reported that the paint has similar chemical compositions to those of the slip. The dissimilarity is that the red paint is composed of more Fe and less Ca. More importantly, it is confirmed that this newly constructed µ-SXRF end-station is able to clearly distinguish the distribution of different elements on the specimen.

3.4. Future work

It is worth mentioning the future development work for this beamline. As mentioned earlier, the Si(111) crystal has been installed in order to select a monochromatic beam of 8 keV from the white X-ray beam. This 8 keV beam will be directed to the diffractometer donated by the Physics Department of King Mongkut's University of Technology, Bangkok, Thailand. This powder X-ray diffraction technique will serve as a

complementary technique to μ-SXRF and others, and the construction is expected to finish by the first half of 2012.

4. Conclusion

A beamline for microbeam XRF using white synchrotron radiation from a bending magnet as an X-ray source has been constructed and successfully installed at the SPL. It has been designed to be integrated into the DXL beamline (*i.e.* BL6: DXL beamline). The beamlines are now called BL6a:DXL and BL6b:XRF/XRD. A data acquisition program using the *LabVIEW* platform has also been developed at SLRI. The beam profile has been measured using a thin wire of copper. It has been found that the beam size is approximately 100 μm. Finally, an elemental distribution of an archaeological sample has been obtained as an example of how this new μ-SXRF end-station can be employed.

We would like to acknowledge the Physics Department, Faculty of Science, King Mongkut's University of Technology Thonbori for the donation of the X-ray diffractometer. We would also like to thank Dr Gema Martinez-Criado and Dr Alejandro Homs Puron from ESRF, France, for valuable advice. We are grateful to Ban Chiang National Museum, Udonthani, Thailand, for providing the sample used in this study.

References

Bilderback, D. H. (2007). *X-ray Spectrom.* **32**, 195–207.
Bubpha, S. (2003). *Bull. Indo-Pac. Prehist. Assoc.* **23**, 15–18.
Dumont, M., Zoeger, N., Streli, C., Wobrauschek, P., Falkenberg, G., Sander, P. M. & Pyzalla, A. R. (2009). *Powder Diffr. J.* **24**, 130–134.
Frisia, S., Borsato, A., Fairchild, I. J. & Susinic, J. (2005). *Earth Planet. Sci. Lett.* **235**, 729–740.
Geraki, K., Farquharson, M. J., Bradley, D. A. & Hugtenburg, R. P. (2004). *Nucl. Instrum. Methods Phys. Res. B*, **213**, 564–568.
Kanngießer, B. & Haschke, M. (2006). *Handbook of Practical X-ray Fluorescence Analysis*, edited by B. Beckhoff, B. Kanngieber, N. Langhoff, R. Wedell and H. Wolff, pp. 442–462. Berlin, Springer-Verlag.
Kempenaersa, L., Vinczea, L. & Janssens, K. (2000). *Spectrochim. Acta B*, **55**, 651–669.
Lengeler, B., Schroer, C. G., Richwin, M. & Tummler, J. (1999). *Appl. Phys. Lett.* **74**, 3924–3926.
McGovern, P. E., Vernon, W. W. & White, J. C. (1985). *MASCA J.* **3**, 104–113.
Sole, V. A., Papillon, E., Cotte, M., Walter, Ph. & Susini, J. (2007). *Spectrochim. Acta B*, **62**, 63–68.
Tanthanuch, W., Pattanasiriwisawa, W., Somphon, W. & Srilomsak, S. (2011). *Suranaree J. Sci. Technol.* **18**, 15–28.
Vries, J. L. de & Vrebos, B. A. R. (2002). *Handbook of X-ray Spectrometry*, 2nd ed., edited by R. E. Van Grieken and A. A. Markovicz, pp. 341–405. New York: Marcel Dekker.
Yanagihara, M. & Yamashita, M. (2004). *X-ray Spectrometry: Recent Technological Advances*, edited by K. Tsuji, J. Injuk and R. Van Grieken, pp. 63–78. West Sussex: John Wiley and Sons.